Acta Oceanol. Sin., 2023, Vol. 42, No. 6, P. 89–99
https://doi.org/10.1007/s13131-022-2143-9
http://www.aosocean.com
E-mail: ocean2@hyxb.org.cn

Hazard risk assessment of tropical cyclones based on joint probability theory

Shanshan Tao[1], Yunfei Hua[1], Sheng Dong[1]*

[1] College of Engineering, Ocean University of China, Qingdao 266100, China

Received 30 July 2022; accepted 27 December 2022

Abstract

The main hazard-causing factors of tropical cyclones are strong wind, heavy rainfall, and storm surge. Evaluation of the hazard-causing degree of a tropical cyclone requires a joint intensity analysis of these hazard-causing factors. According to the maximum hourly mean wind speed, total rainfall, and maximum tide level at various observation stations in Hong Kong during these tropical cyclones, three hazard-causing indices for tropical cyclones are introduced: the strong-wind index (*VI*), total-rainfall index (*RI*), and tide-level index (*LI*). Through a joint probability analysis of *VI*, *RI*, and *LI* for a tropical cyclone affecting Hong Kong, the joint return period is calculated to evaluate its joint hazard-causing intensity. A limit state function of Hong Kong's resistance to tropical cyclones is developed and used to evaluate the regional risk of tropical cyclones affecting Hong Kong. The results indicate that the joint return period of *VI*, *RI*, and *LI* can reflect the joint hazard-causing intensity of strong wind, heavy rain, and storm surge caused by tropical cyclones; if the overall design return periods of the regional structures decrease, the regional ability to defend against tropical cyclone disasters is degraded.

Key words: tropical cyclone, Hong Kong, trivariate copulas, hazard-causing factors, regional risk

Citation: Tao Shanshan, Hua Yunfei, Dong Sheng. 2023. Hazard risk assessment of tropical cyclones based on joint probability theory. Acta Oceanologica Sinica, 42(6): 89–99, doi: 10.1007/s13131-022-2143-9

1 Introduction

A tropical cyclone is a cyclonic vortex that occurs in a tropical or subtropical ocean. Tropical cyclones are often accompanied by strong wind, rainstorm, and storm surge (Houze, 2014; Hoque et al., 2017; Kashem et al., 2019). They are destructive weather systems with high frequencies, wide ranges, and high intensities. Hong Kong is an important commercial port connecting East Asia, Southeast Asia, Australia and the Americas. However, because of its geographical location, it has been affected by tropical cyclone disasters year round, causing significant economic losses (Wang and Zhang, 2018). Therefore, a comprehensive assessment of the hazard-causing intensity of historical tropical cyclones is helpful for the relevant disaster prevention departments to take precautions in advance and reduce losses.

Most natural disasters involve the comprehensive action of multiple hazard-causing factors, and are difficult to fully be characterised the risk grades using a single hazard-causing factor. The main hazard-causing factors of tropical cyclones include strong wind, heavy rainfall, and storm surge (Hendricks, 2012; Yan et al., 2020; Ding et al., 2020). The intensity and frequency of these hazard-causing factors significantly affect the risk grades of tropical cyclones. Strong wind is one of the most important hazard-causing factors of tropical cyclones, as it often causes extensive damage to coastal areas and inland housing, infrastructure, and ecosystems (Kruk et al., 2010; Shao et al. 2018). In many studies, indicators related to wind speed have been used to measure the risk grades of tropical cyclones (Schroeder et al., 2009; Li and Duan, 2010). However, heavy rainfall, storm surge, and other hazard-causing factors cause large numbers of casualties and substantial economic losses (Cerveny and Newman, 2000; Phadke et al., 2003; Bloemendaal et al., 2019). Heavy rainfall often leads to severe urban inland inundation and floods, including flash floods (Czajkowski et al., 2013; Meyer et al., 2014; Yussouf et al., 2020). Storm surge can damage coastal protection facilities, submerge large coastal zones, cause casualties, and significantly affect the surrounding areas (Melton et al., 2010; Sun et al., 2015; Kim et al., 2019; Shi et al., 2020). In the present study, strong wind, heavy rainfall, and storm surge were selected as three representative factors to study the hazard-causing intensity of tropical cyclones.

At present, the comprehensive risk-assessment methods for tropical cyclones mainly include the construction of a comprehensive risk index and multivariate joint probability analysis. According to the intensity, the duration, and other data of tropical cyclones, Xiao et al. (2011) proposed the Tropical Cyclone Potential Impact Index (TCPI) and analysed the interannual variation and spatial distribution of the TCPI from 1949 to 2009. Saha and Wasimi (2014) developed a landfall potential index to reflect the possibility of tropical cyclone landing. Yu et al. (2017) proposed a comprehensive evaluation index for the hazard grades of strong winds and heavy rainfall of tropical cyclones and used it to evaluate the potential hazard grades of tropical cyclones in Southeast China. Chen et al. (2019) defined a joint index based on the wind and precipitation of a tropical cyclone to assess the combined effects of wind and precipitation.

The calculation of the multivariate joint probability is import-

Foundation item: The National Natural Science Foundation of China—Shandong Joint Fund under contract No. U1706226; the National Natural Science Foundation of China under contract No. 52171284.
*Corresponding author, E-mail: dongsh@ouc.edu.cn

ant for accurate assessment of the comprehensive risk of tropical cyclones. Copulas can connect the joint distribution function with their respective marginal distribution functions and are widely used in the comprehensive risk assessment of hazard-causing factors of natural disasters (Tsakiris et al., 2015; Lin-Ye et al., 2017; Radfar et al., 2021). Ye and Fang (2018) used copulas to study the combined wind and rain risk of historical tropical cyclones in coastal areas of China. Hu et al. (2010) used copulas to construct the joint distribution functions of typhoons and plum rain and calculated the probabilities of encountering typhoons and plum rain in the Taihu Lake Basin. Xu et al. (2019) used copulas to study the bivariate return periods of composite events of rainfall and storm surge. In addition, copulas are widely used for analysing sandstorms, droughts, and other natural disasters (Mirabbasi et al., 2012; Li et al., 2013; Liu et al., 2015). At present, most studies on the hazard-causing factors of tropical cyclones only involve bivariate situations, and there have been few studies involving three factors.

In this study, strong wind, rainfall, and storm surge are represented by the maximum hourly mean wind speed (V), total rainfall amount (R) and maximum tide level (L) of the tropical cyclone process, respectively. According to the data of V, R, and L for various observation stations in Hong Kong during the impact periods of 129 historical tropical cyclones from 1997 to 2020, three hazard-causing indices for tropical cyclones affecting Hong Kong are calculated: the strong-wind index (VI), total-rainfall index (RI), and tide-level index (LI). Then, the optimal marginal distribution and trivariate joint probability distribution of VI, RI, and LI are fitted and selected, and the joint return periods of VI, RI, and LI for tropical cyclones are calculated to evaluate the joint hazard-causing intensity. The interannual variation of the trivariate joint return period for 129 historical tropical cyclones is analysed. Finally, by constructing the limit state function of Hong Kong's resistance to tropical cyclones, the regional risk of tropical cyclones affecting Hong Kong is evaluated.

2 Data sources and hazard-causing intensity indices

2.1 *Data sources*

The data of tropical cyclones were obtained from the Tropical Cyclone Annual Publications (Hong Kong Observatory, 1997–2020). The distribution of wind stations, rainfall stations, and tide gauge stations in Hong Kong is shown in Fig. 1. The names of these stations are presented in Table 1. The elevations of the anemometers can refer to the Tropical Cyclone Annual Publications (Hong Kong Observatory, 1997–2020).

If a tropical cyclone enters within 800 km in Hong Kong, the Hong Kong Observatory issues corresponding warning signals (1, 3, 8, 9, and 10, in order of increasing risk) according to the impact of the cyclone on the area (Hong Kong Observatory, 1997–2020). Although tropical cyclones affecting Hong Kong can reach and surpass the typhoon grade during their lifecycle, they may be less intense when they influence Hong Kong, or their path may be far from the Hong Kong area, causing them to have little impact. Thus, it is reasonable to use the warning signals issued by the Hong Kong Observatory and the wind speed observations at various anemometers in Hong Kong (rather than the categories of tropical cyclones) to assess the wind hazard-causing intensity of a tropical cyclone affecting Hong Kong.

The annual tropical cyclone report records two types of wind speeds for each tropical cyclone at each station: the maximum gust peak speed and the maximum hourly mean wind speed. The maximum hourly mean wind speed corresponds to winds averaged over a 60-min interval ending on the hour. It can reflect the hazard-causing intensity of strong winds caused by tropical cyclones.

Rainfall data were obtained from a network of meteorological and rainfall stations operated by the Hong Kong Observatory, as well as rain gauges operated by the Geotechnical Engineering Office. Daily rainfall amounts are computed over a 24-h period end-

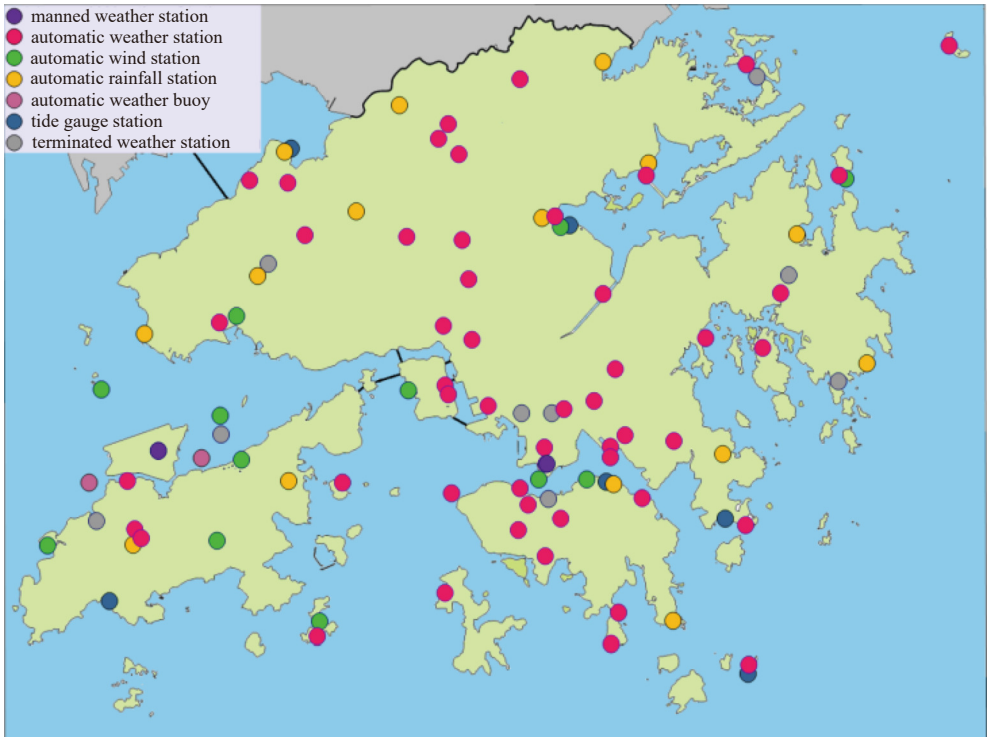

Fig. 1. Distribution of wind, rainfall and tide gauge stations in Hong Kong.

Table 1. Names of wind, rainfall and tide gauge stations in Hong Kong

Wind station	Wind station	Rainfall station
Bluff Head	Ta Kwu Ling	Jordan Valley
Central Pier	Tai Mei Tuk	Kwai Chung
Cheung Chau	Tai Mo Shan	Mid Levels
Cheung Chau Beach	Tai Po Kau	Sha Tin
Green Island	Tap Mun East	Shau Kei Wan
HKIA	Tate's Cairn	Shek Kong
Kai Tak	Tseung Kwan O	So Uk Estate
King's Park	Tsing Yi Shell Oil Depot	Tai Mei Tuk
Lamma Island	TMGO	Tap Shek Kok
Lau Fau Shan	Waglan Island	Tung Chung
Ngong Ping	Wetland Park	TMR
North Point	Wong Chuk Hang	
Peng Chau		**Tide gauge station**
Ping Chau	**Rainfall station**	Quarry Bay
Sai Kung	Hong Kong Observatory	Shek Pik
Sha Chau	HKIA	Tsim Bei Tsui
Sha Lo Wan	Cheung Chau	Tai Miu Wan
Sha Tin	Aberdeen	Tai Po Kau
Shek Kong	Fanling	Waglan Island
Star Ferry	High Island	–

Note: HKIA: Hong Kong International Airport; TMGO: Tuen Mun Government Offices; TMR: Tuen Mun Reservoir. – represents no station.

ing at midnight Hong Kong Time. The total rainfall generated by a tropical cyclone is the sum of all the daily rainfall at a rainfall station during the cyclone. It can reflect the hazard-causing intensity of heavy rain caused by tropical cyclones.

The observations of each tide gauge station include the maximum sea tide level (above chart datum) and the maximum storm surge (above astronomical tide) during the tropical cyclone. The maximum tide level can reflect the hazard-causing intensity of storm surge caused by tropical cyclones.

There are many wind stations, rainfall stations, and tide gauge stations in Hong Kong. For a given tropical cyclone, the maximum hourly mean wind speed, total rainfall, and maximum sea level differ among the stations.

2.2 *Hazard-causing intensity indices*

The joint hazard-causing intensity of the tropical cyclone mainly refers to the intensity, total amount and area of wind, rainfall, and storm surge caused by the tropical cyclone. Tropical cyclones cause strong wind, flood, or storm surge in the landing area and surrounding areas. For each tropical-cyclone hazard-causing factor, its intensity and scope should be considered. The damage caused by a tropical cyclone to different areas of Hong Kong varies significantly; thus, the data of wind speed, rainfall, and tidal level differ among different stations. Therefore, the *V*, *R*, or *L* of a single observation station during the impact period of a tropical cyclone is insufficient to reflect the hazard-causing intensity for the entire Hong Kong region. Hence, it is necessary to develop a comprehensive *VI*, *RI*, and *LI* covering different observation stations (Chen et al., 2009).

In this study, comprehensive hazard-causing intensity indices *VI*, *RI*, and *LI* are calculated using the data of *V*, *R*, and *L* for various observation stations in Hong Kong during the impact periods of 129 historical tropical cyclones from 1997 to 2020. These indices take into account the average of multiple tropical cyclones over many years, as well as the average and extreme values of the current tropical cyclone for different stations. They are defined as follows.

2.2.1 *Strong-wind index*

Before calculating the comprehensive hazard-causing intensity index of strong wind *VI*, the power law is used to unify the wind data. Because the anemometers of different weather stations are at different elevations, it is necessary to normalise the elevations to 10 m using Eq. (1).

$$V = V_1 \times \left(\frac{z}{z_1}\right)^m, \tag{1}$$

where V and V_1 represent the wind speeds at heights z and z_1 above the ground, respectively, and m is the power exponent, which is determined by the characteristics of underlying surface (it is generally between 1/2 and 1/8).

According to the geomorphological characteristics of Hong Kong and the surrounding environments of the stations, the woodland case is taken as the general performance of this area; thus, m is set as 0.28.

The hazard-causing intensity index of strong wind *VI* for a tropical cyclone is mainly measured by the maximum hourly mean wind speed for different wind stations. For the *i*th tropical cyclone, VI_i is defined as follows:

$$VI_i = \sum_{j=1}^{n_i} V_{ij}/(n_i \cdot AV) \times [1 + (T_{8i} + T_{10i})/T_i]^2, \tag{2}$$

$$AV = \sum_{i=1}^{m} \left(\sum_{j=1}^{n_i} V_{ij}/n_i\right)/m, \tag{3}$$

where V_{ij} represents the maximum hourly mean wind speed of the *i*th tropical cyclone at the *j*th wind station, n_i represents the number of wind stations during the impact period of the *i*th tropical cyclone, m represents the total number of historical tropical cyclones affecting Hong Kong (for example, there were 129 tropical cyclones affecting Hong Kong between 1997 and 2020), T_{8i} represents the duration of the *i*th tropical cyclone beyond warning signal 8, T_{10i} represents the duration of the *i*th tropical cyclone beyond warning signal 10, T_i represents the total duration of the *i*th tropical cyclone affecting Hong Kong, and AV represents the average of the maximum hourly mean wind speeds at different wind stations during multiple historical tropical cyclones.

The strong-wind index *VI* is a dimensionless ratio obtained by dividing the average of the maximum hourly mean wind speeds at the wind stations during the impact period of a tropical cyclone by the average of all historical averages, taking into account extreme cases of strong or gale winds with warning signals of $\geqslant 8$ and 10.

2.2.2 *Total-rainfall index*

The hazard-causing intensity index of heavy rainfall *RI* for a tropical cyclone is mainly measured by the total rainfall amount for different rainfall stations. For the *i*th tropical cyclone, RI_i is defined as follows:

$$RI_i = \sum_{j=1}^{n_i} R_{ij}/(n_i \cdot AR) \times [1 + (T_{50i} + T_{100i})/T_i]^2, \tag{4}$$

$$AR = \sum_{i=1}^{m}\left(\sum_{j=1}^{n_i} R_{ij}/n_i\right)/m, \tag{5}$$

where R_{ij} represents the total rainfall amount of the ith tropical cyclone at the jth rainfall station, n_i represents the number of rainfall stations during the impact period of the ith tropical cyclone, m represents the total number of historical tropical cyclones affecting Hong Kong, T_{50i} represents the number of days in which the daily rainfall exceeds 50 mm, T_{100i} represents the number of days in which the daily rainfall exceeds 100 mm, T_i represents the total number of days with rainfall during the impact period of the tropical cyclone affecting Hong Kong, and AR represents the average of the total rainfall amount at different rainfall stations during multiple historical tropical cyclones.

The heavy-rainfall index RI is a dimensionless ratio obtained by dividing the average of the total rainfall amounts at the stations during the impact period of a tropical cyclone by the average of all historical averages, taking into account extreme cases of heavy rain with daily rainfall above 50 mm and 100 mm.

2.2.3 *Tide-level index*

The hazard-causing intensity index of storm surge LI for a tropical cyclone is mainly measured by the maximum tide level for different tide gauge stations. For the ith tropical cyclone, LI_i is defined as follows:

$$LI_i = \sum_{j=1}^{n_i} L_{ij}/(n_i \cdot AL) \times \left[1 + \sum_{k=1}^{\tilde{n}_i}\left(L_{i(k)} - AL\right)/(n_i \cdot AL)\right]^2, \tag{6}$$

$$AL = \sum_{i=1}^{m}\left(\sum_{j=1}^{n_i} L_{ij}/n_i\right)/m, \tag{7}$$

where L_{ij} represents the maximum tide level of the ith tropical cyclone at the jth tide gauge station, n_i represents the number of tide gauge stations during the impact period of the ith tropical cyclone, m represents the total number of historical tropical cyclones affecting Hong Kong, AL represents the average of the maximum tide levels at different tide gauge stations during multiple historical tropical cyclones, $\tilde{n}_i$ represents the number of tide gauge stations in L_{ij} that exceed AL during the impact period of the ith tropical cyclone, and $L_{i(k)}$ represents the maximum tide level that exceeds the AL of the ith tropical cyclone at the kth tide gauge station.

The tide-level index LI is a dimensionless ratio obtained by dividing the average of the maximum tide levels at the stations during the impact period of a tropical cyclone by the average of all historical averages, taking into account extreme cases of a high tide level exceeding AL.

3 Methodology

According to the joint probability distribution of hazard-causing indices VI, RI, and LI, the joint hazard-causing intensity of the ith tropical cyclone can be defined by using the joint return period of its indices VI_i, RI_i, and LI_i. To obtain the joint probability distributions of VI, RI, and LI, Gumbel, Weibull, Pearson type 3 (P-III) and lognormal distributions are used to fit the best marginal distributions of VI, RI, and LI. Then, the Gaussian, Gumbel–Hougaard (G-H), Clayton, and Frank copulas are used to construct the joint distribution, and the Kolmogorov–Smirnov (K-S) test and Akaike information criterion (AIC) are used to select the best trivariate probability model.

3.1 *Marginal probability models*

The cumulative probability distribution functions, i.e., $F(x)$, of the Gumbel distribution, three-parameter Weibull distribution, P-III distribution, and three-parameter lognormal distribution are given by Eqs (8)–(11), respectively.

$$F(x) = \exp\left\{-\exp\left[-\alpha\left(x-\mu\right)\right]\right\}, \tag{8}$$

$$F(x) = 1 - \exp\left[-\left(\frac{x-\mu}{\sigma}\right)^{\gamma}\right],\ x \geqslant \mu, \tag{9}$$

$$F(x) = \int_a^x \frac{\beta_0^{\alpha}}{\Gamma(\alpha)} \cdot (t-\mu)^{\alpha-1} \exp\left[-\beta_0\left(t-\mu\right)\right] \mathrm{d}t, t \geqslant \mu, \alpha > 0, \tag{10}$$

$$F(x) = \int_a^x \frac{1}{(t-a)\sigma\sqrt{2\pi}} \cdot \exp\left\{-\frac{1}{2\sigma^2}\left[\ln\left(t-a\right)-\mu\right]^2\right\} \mathrm{d}t, t > a, \tag{11}$$

where μ and a are the location parameters; α (in Eq. (8)), β_0 and σ are the scale parameters; α (in Eq. (10)) and γ are the shape parameters.

3.2 *Trivariate copula*

A copula is a function that describes multivariate distributions defined on the unit hypercube, and the univariate marginal distributions are uniform on the interval (0, 1). According to Sklar (1959) theorem, if the marginal probability functions $F_X(x) = P(X \leqslant x)$, $F_Y(y) = P(Y \leqslant y)$, and $F_Z(z) = P(Z \leqslant z)$ of random variables X, Y, and Z are known, the joint distribution function $F_{XYZ}(x, y, z)$ can be obtained as follows:

$$\begin{aligned} F_{XYZ}(x,y,z) =& P\left(X \leqslant x, Y \leqslant y, Z \leqslant z\right) = \\ & C\left(F_X(x), F_Y(y), F_Z(z)\right) = C(u, v, w), \end{aligned} \tag{12}$$

where X, Y, and Z represent the attributes of the event (corresponding to VI, RI, and LI, respectively, in this study); x, y, and z represent the thresholds of the attributes; u, v, and w represent the marginal probability functions of the attribute.

In addition, if the probability density functions $f_X(x)$, $f_Y(y)$, and $f_Z(z)$ exist, the joint probability density function $f_{XYZ}(x, y, z)$ of X, Y, and Z can be expressed as

$$\begin{aligned} f_{XYZ}(x,y,z) =& c\left(F_X(x), F_Y(y), F_Z(z)\right) f_X(x) f_Y(y) f_Z(z) = \\ & c\left(u, v, w\right) f_X(x) f_Y(y) f_Z(z), \end{aligned} \tag{13}$$

where $c(u, v, w)$ is defined as

$$c(u,v,w) = \frac{\partial^3 C(u,v,w)}{\partial u \partial v \partial w}, \tag{14}$$

where $c(u, v, w)$ represents the joint probability density functions calculated using the copulas.

The commonly used trivariate copulas are the Gaussian, G-H, Clayton, and Frank copulas, and their joint probability distribution functions and joint density functions are presented below.

(1) Gaussian copula

$$C(u,v,w;\boldsymbol{\Sigma}) = \int_{-\infty}^{\Phi^{-1}(u)}\int_{-\infty}^{\Phi^{-1}(v)}\int_{-\infty}^{\Phi^{-1}(w)} \frac{1}{(2\pi)^{\frac{3}{2}}|\boldsymbol{\Sigma}|^{\frac{1}{2}}}\times \exp\left(-\frac{1}{2}\boldsymbol{\omega}^{\mathrm{T}}\boldsymbol{\Sigma}^{-1}\boldsymbol{\omega}\right)\mathrm{d}\omega, \tag{15}$$

$$c(u,v,w;\boldsymbol{\Sigma}) = \frac{1}{|\boldsymbol{\Sigma}|^{\frac{1}{2}}}\exp\left[-\frac{1}{2}\left(\boldsymbol{\zeta}^{\mathrm{T}}\boldsymbol{\Sigma}^{-1}\boldsymbol{\zeta}-\boldsymbol{\zeta}^{\mathrm{T}}\boldsymbol{\zeta}\right)\right]. \tag{16}$$

Here, $\Phi^{-1}(\cdot)$ represents the inverse of the standard normal distribution, and Σ represents the correlation coefficient matrix, which is defined as

$$\boldsymbol{\Sigma} = \begin{pmatrix} 1 & \rho_{12} & \rho_{13} \\ \rho_{21} & 1 & \rho_{23} \\ \rho_{31} & \rho_{32} & 1 \end{pmatrix};\ \rho_{ij}=\rho_{ji},\ i\neq j;\ -1\leqslant\rho_{ij}\leqslant 1. \tag{17}$$

Additionally, $\boldsymbol{\omega} = [\omega_1, \omega_2, \omega_3]^{\mathrm{T}}$ represents the integrand variable matrix, and $\boldsymbol{\zeta} = [\Phi^{-1}(u), \Phi^{-1}(v), \Phi^{-1}(w)]^{\mathrm{T}}$.

(2) G-H copula

$$C(u,v,w;\theta) = \exp\left\{-\left[(-\ln u)^{\theta}+(-\ln v)^{\theta}+(-\ln w)^{\theta}\right]^{\frac{1}{\theta}}\right\},\ \theta\in[1,+\infty), \tag{18}$$

where θ is the correlated parameter.

$$c(u,v,w;\theta) = \frac{(-\ln u\ln v\ln w)^{\theta-1}}{uvw}\exp\left(-\omega^{\frac{1}{\theta}}\right)\times \left[\omega^{\frac{3}{\theta}-3}+(3\theta-3)\,\omega^{\frac{2}{\theta}-3}+(\theta-1)(2\theta-1)\,\omega^{\frac{1}{\theta}-3}\right], \tag{19}$$

where $\omega = (-\ln u)^{\theta}+(-\ln v)^{\theta}+(-\ln w)^{\theta}$.

(3) Clayton copula

$$C(u,v,w;\theta) = \left(u^{-\theta}+v^{-\theta}+w^{-\theta}-2\right)^{-\frac{1}{\theta}},\theta\in(0,\infty), \tag{20}$$

$$c(u,v,w;\theta) = u^{-(\theta+1)}v^{-(\theta+1)}w^{-(\theta+1)}(1+\theta)(1+2\theta)\times \left(u^{-\theta}+v^{-\theta}+w^{-\theta}-2\right)^{-\left(\frac{1}{\theta}+3\right)}. \tag{21}$$

(4) Frank copula

$$C(u,v,w;\theta) = -\frac{1}{\theta}\ln\left[1+\frac{\left(\mathrm{e}^{-\theta u}-1\right)\left(\mathrm{e}^{-\theta v}-1\right)\left(\mathrm{e}^{-\theta w}-1\right)}{\left(\mathrm{e}^{-\theta}-1\right)^2}\right],\theta\neq 0 \tag{22}$$

$$c(u,v,w;\theta) = \frac{\theta^2\mathrm{e}^{-\theta u}\mathrm{e}^{-\theta v}\mathrm{e}^{-\theta w}\left(\mathrm{e}^{-\theta}-1\right)^2\left[\left(\mathrm{e}^{-\theta}-1\right)^2-\left(\mathrm{e}^{-\theta u}-1\right)\left(\mathrm{e}^{-\theta v}-1\right)\left(\mathrm{e}^{-\theta w}-1\right)\right]}{\left[\left(\mathrm{e}^{-\theta}-1\right)^2+\left(\mathrm{e}^{-\theta u}-1\right)\left(\mathrm{e}^{-\theta v}-1\right)\left(\mathrm{e}^{-\theta w}-1\right)\right]^3}. \tag{23}$$

3.3 *Estimation of parameters, goodness of fit, and copula selection*

In this study, the maximum likelihood method is used to estimate both marginal distributions and trivariate joint probability distributions, and the K-S test is used to judge whether the parameter estimation of univariate curves and copulas satisfies the requirements. The choice of the optimal models is mainly based on the average sum of deviation squares and the AIC.

The K-S test is a robust goodness-of-fit test method for determining whether samples obey the selected model. The statistic of the K-S test is

$$D_n = \max_{1\leqslant i\leqslant n}\left|\hat{F}_i - F_i\right|, \tag{24}$$

where $\hat{F}_i$ represents the empirical frequency, and F_i represents the theoretical frequency. When D_n is smaller than the critical value $D_n(\alpha)$, the selected model has passed the fitting test.

The AIC value is a commonly used standard for evaluating model fit. It is defined as follows:

$$\mathrm{AIC} = n\ln(\mathrm{MSE}) + 2k, \tag{25}$$

where n represents the length of the sample, k represents the number of probability model parameters, and MSE represents the mean squared error, which is defined as

$$\mathrm{MSE} = \frac{1}{n}\sum_{i=1}^{n}\left(\hat{F}_i - F_i\right)^2. \tag{26}$$

A smaller AIC value corresponds to a better fitting effect of the joint probability distribution model.

3.4 *Joint return periods*

The joint return period of a trivariate characterised event can be described in $RP_{\cap}$, which is defined as the return period of an event with three variables all above a specific threshold ($X\geqslant x$, $Y\geqslant y$, and $Z\geqslant z$). The joint return period is expressed as follows:

$$RP_{\cap} = \frac{E(t)}{P(X\geqslant x, Y\geqslant y, Z\geqslant z)} = \frac{E(t)}{\int_x^{+\infty}\int_y^{+\infty}\int_z^{+\infty} f_{XYZ}(x,y,z)\mathrm{d}x\mathrm{d}y\mathrm{d}z} = \frac{E(t)}{\int_x^{+\infty}\int_y^{+\infty}\int_z^{+\infty} c(u,v,w)f_X(x)f_Y(y)f_Z(z)\mathrm{d}x\mathrm{d}y\mathrm{d}z} = \frac{E(t)}{\int_u^1\int_v^1\int_w^1 c(u,v,w)\mathrm{d}u\mathrm{d}v\mathrm{d}w}, \tag{27}$$

where, for the ith tropical cyclone, x, y, and z represent VI_i, RI_i, and LI_i, respectively; $E(t)$ represents the mean interval between two successive tropical cyclones (in this study, a total of 129 tropical cyclones occurred between 1997 and 2020; thus, $E(t)$ = 24/129).

4 Joint hazard-causing intensity analysis

4.1 *Fittings of marginal distribution*

First, the *VI*, *RI*, and *LI* of each tropical cyclone affecting Hong Kong from 1997 to 2020 were selected and fitted by the Gumbel, Weibull, P-III, and lognormal distributions. The data sequences are shown in Fig. 2, and the fitting results are presented in Table 2 and Fig. 3.

Because the index *RI* has zero-value data, the zero-value sequences are ignored first, and the frequency of nonzero-value sequences $P(Y \leqslant y \,|\, Y > 0)$ is calculated. Then, the frequency of sequences containing zero values $P(Y \leqslant y)$ is calculated according to the following total probability formula:

$$P(Y \leqslant y) = 1 - \frac{n}{N} + \frac{n}{N} P(Y \leqslant y \,|\, Y > 0)\,, \tag{28}$$

where n represents the number of $Y > 0$ values in the sequence, and N represents the total number of values in the sequence.

The results in Table 2 indicate that at a confidence level of 0.05, the four distributions of *VI* all pass the K-S tests. The Q (sum of squares of deviation) values of the distributions increase in the following order: lognormal distribution, P-III distribution, Gumbel distribution, and Weibull distribution. As shown in Fig. 3, the fitting effect of the lognormal distribution on the upper tail and lower tail is slightly better than those of the other distributions. Therefore, the lognormal distribution function is the optimal fitting function for the marginal distribution of *VI*.

Similarly, the P-III and lognormal distribution functions are selected as the optimal fitting functions of the indices *RI* and *LI*, respectively.

4.2 *Joint probability analysis of VI, RI, and LI*

According to the foregoing optimisation results, the marginal probability distributions of *VI* and *LI* are both lognormal distributions, the marginal probability distribution of *RI* is a P-III dis-

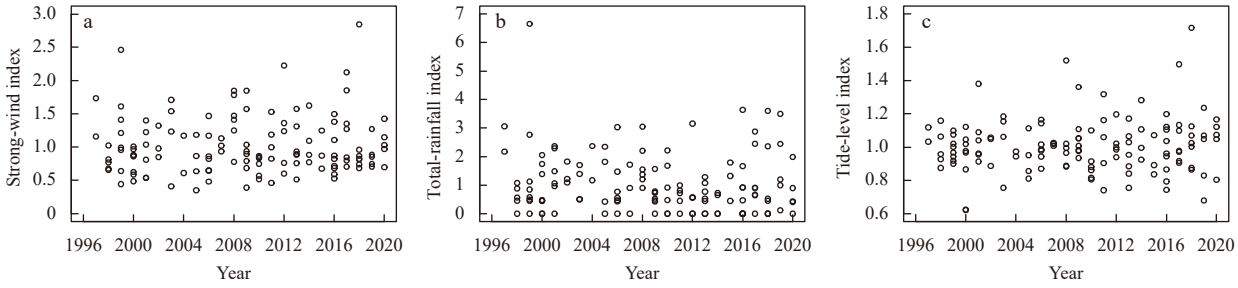

Fig. 2. Scatter plots of hazard-causing intensity indices strong-wind index, total-rainfall index and tide-level index.

Table 2. Parameter estimation and fitting results

Indices	Type	A_1	A_2	A_3	$D_n(0.05)$	$\hat{D}_n$	Q
Strong-wind index	Gumbel	0.830	3.202	–	1.197×10^{-1}	8.096×10^{-2}	7.077×10^{-4}
	Weibull	0.346	0.750	1.619	1.197×10^{-1}	7.185×10^{-2}	9.110×10^{-4}
	P-III	2.233	3.469	0.373	1.197×10^{-1}	5.553×10^{-2}	5.035×10^{-4}
	Lognormal	0.157	–0.266	0.486	1.197×10^{-1}	5.607×10^{-2}	4.017×10^{-4}
Total-rainfall index	Gumbel	0.904	1.607	–	1.347×10^{-1}	1.255×10^{-1}	3.926×10^{-3}
	Weibull	0.118	1.293	1.285	1.347×10^{-1}	1.268×10^{-1}	1.854×10^{-3}
	P-III	0.956	0.976	0.330	1.347×10^{-1}	7.837×10^{-2}	7.015×10^{-4}
	Lognormal	0.109	–0.134	0.868	1.347×10^{-1}	9.940×10^{-2}	8.670×10^{-4}
Tide-level index	Gumbel	0.932	6.892	–	1.197×10^{-1}	9.046×10^{-2}	2.268×10^{-3}
	Weibull	0.598	0.458	2.602	1.197×10^{-1}	8.894×10^{-2}	2.296×10^{-3}
	P-III	4.183	12.718	0.678	1.197×10^{-1}	8.644×10^{-2}	1.715×10^{-3}
	Lognormal	–0.187	0.168	0.131	1.197×10^{-1}	6.826×10^{-2}	8.945×10^{-4}

Note: $\hat{D}_n$ is the K-S stastic, $D_n(0.05)$ is the K-S tests value, Q is the average sum of deviation squares; the corresponding relationship of the parameters is as follows: (1) Gumbel distribution, A_1 and A_2 represent location parameter u and scale parameter α respectively; (2) Weibull distribution, A_1, A_2 and A_3 represent the position parameter μ, shape parameter σ and scale parameter γ, respectively; (3) P-III distribution, A_1, A_2 and A_3 represent α, scale parameter β_0 and μ, respectively; (4) lognormal distribution, A_1, A_2 and A_3 represent the parameters a, μ and σ, respectively. – represents no data.

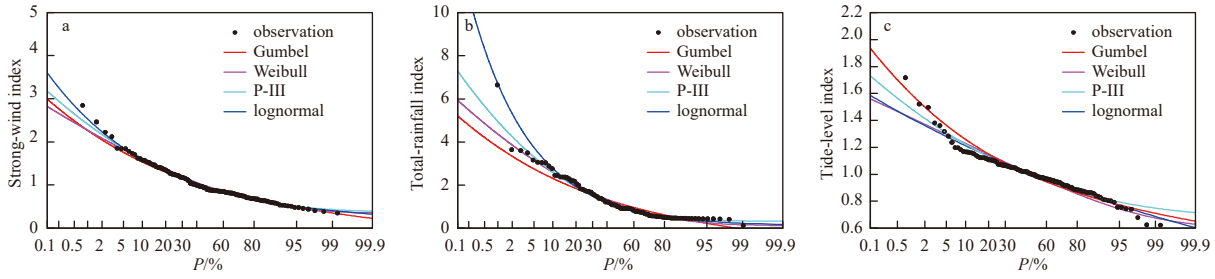

Fig. 3. Data fittings of strong-wind index, total-rainfall index, and tide-level index. P-III represents Pearson type 3.

tribution. The parameter estimation results are presented in Table 2.

On the basis of the univariate marginal distributions $u = F_X(x)$, $v = F_Y(y)$, and $w = F_Z(z)$, the trivariate Gaussian, G-H, Clayton, and Frank copulas $C(u, v, w)$ are used to construct the joint probability distributions of (VI, RI, LI). Then, the optimal trivariate distribution is selected, and the joint return period of (VI, RI, LI) is calculated.

According to the K-S tests and AIC values, the optimal trivariate copula model is selected. The results are presented in Table 3. All the copula models pass the K-S tests, and the G-H copula is the best, as it has the smallest AIC value.

According to Eq. (27), the joint return periods $RP_{\cap}$ are calculated. The joint return periods for the historical tropical cyclones from 1997 to 2020 are shown in Fig. 4.

As shown in Fig. 4, the joint return periods of most tropical cyclones' indices (VI_i, RI_i, LI_i) are <30 a. Typhoon Sam (1999), Typhoon York (1999), Typhoon Hagupit (2008), Severe Typhoon Vicente (2012), Super Typhoon Hato (2017), and Super Typhoon Mangkhut (2018) have joint return periods of >30 a; the corresponding joint return periods are 193 a, 35 a, 131 a, 30 a, 115 a, and 2 274 a, respectively.

Among these tropical cyclones, Mangkhut (2018) has the largest VI_i and LI_i values. Mangkhut does not have the largest RI_i, but it has the longest joint return period. Typhoon Sam (1999) has a VI_i of 1.609, ranking 12th in the dataset, an RI_i of 6.650 (ranking 1st), and an LI_i of 1 (ranking 11th). Its joint return period is ranked 2nd. Typhoon Hagupit (2008) has a wind index VI_i of 1.846 (ranking 7th), a RI_i of 1.207 (ranking 41st), and a LI_i of 1.520 (ranking 2nd). Its joint return period is ranked 3rd.

The joint return periods of York, Vicente, and Hato are also relatively long. Their hazard-causing intensity indices VI_i, RI_i, and LI_i are not the largest but are relatively large. The combination of VI, RI, and LI influences the joint return periods of tropical cyclones, which reflect their comprehensive hazard-causing intensity.

Table 3. Fitting results based on Copula function

Copula function	$\hat{\theta}$	$\hat{D}_n$	$D_n(0.5)$	AIC
Frank	2.049 7	0.101 0	0.119 7	−872.328 0
Clayton	0.339 2	0.084 5	0.119 7	−876.635 0
G-H	1.201 8	0.079 5	0.119 7	−927.422 8
Gaussian	(0.406 5, 0.491 3, −0.017 3)	0.110 8	0.119 7	−856.054 4

Note: AIC: Akaike information criterion.

4.3 *Interannual variations of hazard-causing intensity for tropical cyclones*

To study the interannual variations of the comprehensive hazard-causing intensity for tropical cyclones, the joint return periods of historical tropical cyclones are analysed. Typhoon Mangkhut (2018) is excluded, because as shown in Fig. 4a, it has a significantly longer joint return period than the other tropical cyclones and can be seen as an abnormal tropical cyclone. The mean value of the joint return periods of other tropical cyclones in 2018 is substituted for the joint return period of Mangkhut.

The hazard-causing intensity of tropical cyclones each year is defined by the sum of the joint return periods of all the tropical cyclones in the year. Figure 5a presents the annual change in the hazard-causing intensity (red line) and the total number (blue line) of tropical cyclones. As shown, there is no significant change in the number of tropical cyclones per year; the annual hazard-causing intensity of tropical cyclones exhibits obvious periodic change, and the period is approximately 9 a. If Typhoon Mangkhut is not taken into account, the peak value of the annual hazard-causing intensity of tropical cyclones in each cycle exhibits a decreasing trend.

Additionally, the average hazard-causing intensities of tropical cyclones in 3 a or 6 a are calculated (defined as the sum of annual hazard-causing intensities of all tropical cyclones in 3 a or 6 a). The trend change of the hazard-causing intensity of tropical cyclones can be analysed by this moving average, as shown in Figs 5b and c. In Fig. 5c, the return period in the first 12 a exhibits a decreasing trend, and the return period in the last 6 a exhibits

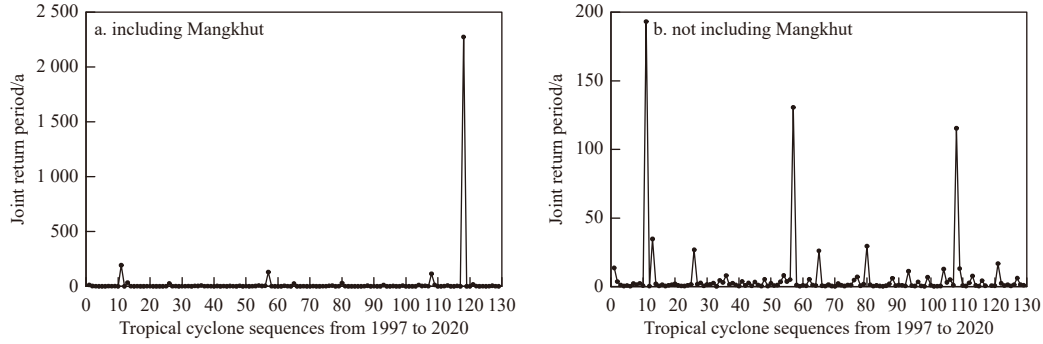

Fig. 4. Joint return periods of strong-wind index (VI), total-rainfall index (RI), and tide-level index (LI).

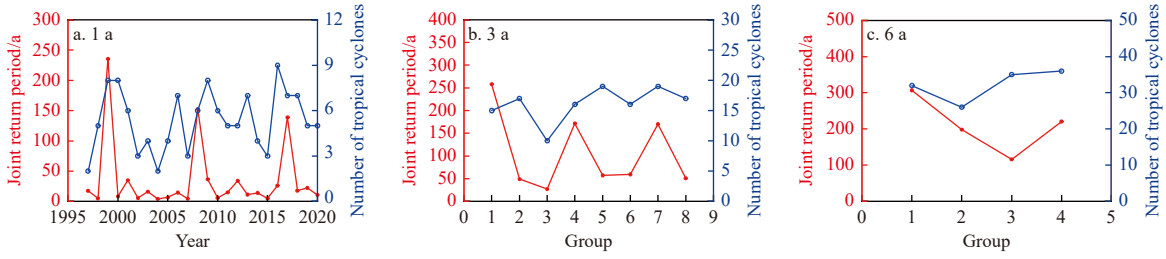

Fig. 5. Interannual variations of the joint return periods (1 a, 3 a and 6 a). The annual change of tropical cyclones in the hazard-causing intensity shows in red line and the total number shows in blue line.

an increasing trend. If Typhoon Mangkhut is taken into account, the increasing trend becomes more significant.

In addition, the maximum joint return period of the all tropical cyclones in each year is extracted to represent the highest hazard-causing intensity of tropical cyclones in the year, as shown in Fig. 6. Additionally, the average joint return period of all tropical cyclones in each year (i.e., the sum of the joint return periods divided by the number of tropical cyclones in the year) is extracted to represent the average hazard-causing intensity of tropical cyclones in the current year, as shown in Fig. 7.

Similar to Fig. 5a, Figs 6 and 7 show that the maximum and average annual hazard-causing intensities of tropical cyclones also have a 9-a cycle. Without consideration of Typhoon Mangkhut, the maximum value of each cycle exhibits a decreasing trend.

5 Regional risk assessment

Hong Kong is frequently affected by tropical cyclones; thus, it is necessary to assess the overall risk of tropical cyclones in this region. In this section, it is assumed that in the structural design of Hong Kong, the design values satisfy the corresponding return period standard of the strong-wind index, total-rainfall index, or tide-level index, and the limit state function of the regional risk to tropical cyclones can be constructed accordingly. According to the joint probability distribution of the hazard-causing intensity indices *VI*, *RI*, and *LI* of tropical cyclones, a regional risk assessment of tropical cyclones affecting Hong Kong is performed.

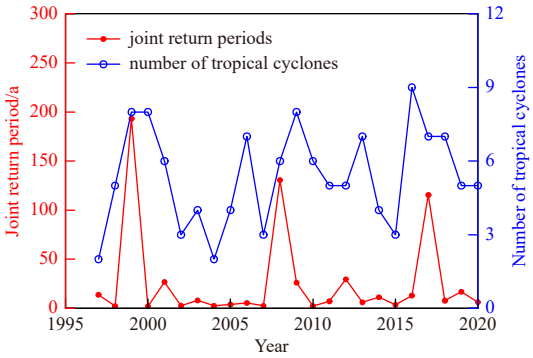

Fig. 6. The annual extremum of the joint return period.

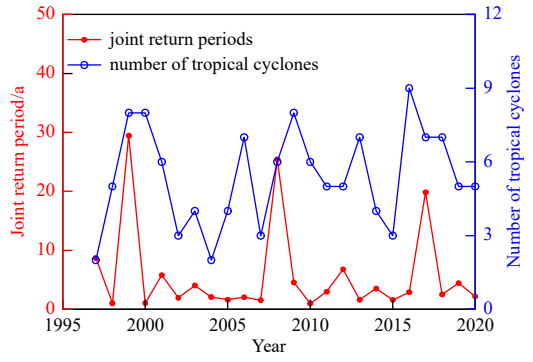

Fig. 7. The annual mean of the joint return period.

5.1 *Return values of indices VI, RI, and LI*

According to the foregoing calculation results, the optimal marginal curves of *VI*, *RI*, and *LI* follow lognormal, P-III, and lognormal distributions, respectively, and corresponding parameter estimations are presented in Table 2. The return values x_T of *VI*, *RI*, or *LI* can be calculated as follows:

$$T = \frac{E(t)}{P(X \geqslant x_T)} = \frac{E(t)}{1 - F(x_T)} \Rightarrow x_T = F^{-1}\left(1 - \frac{E(t)}{T}\right), \quad (29)$$

where X is a random variable (*VI*, *RI*, or *LI*), T represents the return period, x represents the T-year return value, $F(x)$ represents the probability distribution function of X, $E(t)$ represents the mean time interval between two successive tropical cyclones (in this study, a total of 129 tropical cyclones occurred between 1997 and 2020; thus, $E(t)$ can be estimated as 24/129).

The estimated return values of the indices *VI*, *RI*, and *LI* under different return periods are presented in Table 4.

5.2 *Limit state function of regional resistance to tropical cyclones*

According to the hazard-causing intensity indices *VI*, *RI*, and *LI* of tropical cyclones and the assumed return values V, R, and L for structural design in Hong Kong, the limit state function of the hazard-causing factors (strong wind, heavy rainfall, and storm surge) is constructed as follows:

$$Z = 1 - \left(a_1 \frac{VI}{V_{T_1}} + a_2 \frac{RI}{R_{T_2}} + a_3 \frac{LI}{L_{T_3}}\right), \quad (30)$$

where a_1, a_2, and a_3 are linear coefficients of *VI*, *RI*, and *LI*, respectively, and $a_1 + a_2 + a_3 = 1$; V_{T_1} represents the T-year return value of *VI*; R_{T_2} represents the T_2-year return value of *RI*; L_{T_3} represents the T_3-year return value of *LI*; and Z represents the limit state function for *VI*, *RI*, and *LI*.

Under the condition that the return values V, R, and L are known, according to the joint probability distribution of *VI*, *RI*, and *LI* for tropical cyclones, the regional reliability under tropical cyclones affecting Hong Kong can be calculated as

$$P_s = P(Z>0) = \iiint_{Z>0} f_{XYZ}(x,y,z)\mathrm{d}x\mathrm{d}y\mathrm{d}z, \quad (31)$$

where Z represents the limit state function about *VI*, *RI*, and *LI* in Eq. (30); $f(x, y, z)$ represents the joint probability density function of *VI*, *RI*, and *LI*; and P_s represents the regional risk reliability under tropical cyclones affecting Hong Kong.

The reliability P_s can be determined via the direct integration method using the following formula:

$$\begin{aligned} P_s &= \iiint_{Z>0} f_{XYZ}(x,y,z)\mathrm{d}x\mathrm{d}y\mathrm{d}z = \iiint_{R^3} I[Z(x,y,z)] \times \\ & f_{XYZ}(x,y,z)\mathrm{d}x\mathrm{d}y\mathrm{d}z \approx \int_{a_1}^{b_1}\int_{a_2}^{b_2}\int_{a_3}^{b_3} I[Z(x,y,z)] \times \\ & f_{XYZ}(x,y,z)\mathrm{d}x\mathrm{d}y\mathrm{d}z \approx \sum_{i_1=1}^{k_1}\sum_{i_2=1}^{k_2}\sum_{i_3=1}^{k_3} I[Z(a_{1i_1}, a_{2i_2}, a_{3i_3})] \times \\ & f_{XYZ}(a_{1i_1}, a_{2i_2}, a_{3i_3})\Delta a_{1i_1}\Delta a_{2i_2}\Delta a_{3i_3}, \end{aligned} \quad (32)$$

Table 4. Return values of strong-wind index (*VI*), total-rainfall index (*RI*), and tide-level index (*LI*)

Return period/a	10	25	50	100	120	200
Strong-wind index (*VI*)	2.266 7	2.660 0	2.971 3	3.295 8	3.383 4	3.634 3
Total-rainfall index (*RI*)	4.313 9	5.244 8	5.949 8	6.655 4	6.841 1	7.361 4
Tide-level index (*LI*)	1.367 2	1.440 4	1.492 7	1.542 8	1.555 7	1.591 2

where k_1 k_2 and k_3 represent the number of partitions dividing the intervals $[a_1, b_1]$, $[a_2, b_2]$, and $[a_3, b_3]$ into intercells, respectively; a_{ji_j} represents any value in the ith intercell of $[a, b]$, and Δa_{ji_j} represents its length; and $I(\cdot)$ represents the indicative function, i.e.,

$$I[Z(x,y,z)] = \begin{cases} 1, & Z(x,y,z) < 0 \\ 0, & Z(x,y,z) > 0 \end{cases}. \tag{33}$$

The upper and lower limits of the integral a and b can be determined using the following formula:

$$\int_a^b f(x)\mathrm{d}x \geqslant 1 - \varepsilon_0, \tag{34}$$

where ε represents the calculation accuracy.

The β can be calculated using the regional reliability P_s.

$$\beta = -\Phi^{-1}(1 - P_s), \tag{35}$$

where $\Phi^{-1}(\cdot)$ represents the inverse function of the standard normal distribution.

5.3 *Regional risk index of tropical cyclones affecting Hong Kong*

Assume that the return periods T_1, T_2, and T_3 in Eq. (30) are identical, e.g., $T = T_1 = T_2 = T_3 = 100$ a. As the linear coefficient combination (a_1, a_2, a_3) in Eq. (30) changes, the β can be calculated according to Eqs (30), (32), and (35), as shown in Table 5 and Fig. 8. The regional risk reliability index can reflect the change in regional reliability with the change in regional attention (a_1, a_2, a_3) to the strong wind, heavy rainfall, or storm surge caused by tropical cyclones under the condition that the overall structural design of Hong Kong considers the return periods of the hazard-causing indices *VI*, *RI*, and *LI*.

Assume that the return periods T_1, T_2, and T_3 in Eq. (30) have the same values, e.g., $T = T_1 = T_2 = T_3 = 50$ a. As the linear coefficient combination (a_1, a_2, a_3) in Eq. (30) changes, the β can be calculated, as shown in Table 6 and Fig. 9.

As indicated by Tables 5 and 6, if the return periods of the overall design of the regional structures decrease, the regional ability to defend against tropical cyclone disasters (i.e., regional risk reliability) decreases.

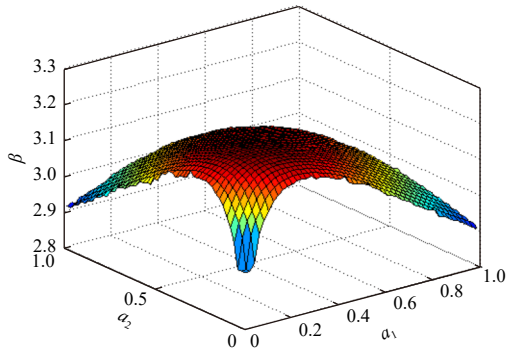

Fig. 8. Regional risk reliability index (T = 100 a).

Table 5. Regional risk reliability index (T = 100 a)

a_1	a_2										
	0	0.1	0.2	0.3	0.4	0.5	0.6	0.7	0.8	0.9	1.0
0	2.958 2	3.111 4	3.168 5	3.165 4	3.147 8	3.116 7	3.069 2	3.031 9	2.992 0	2.944 8	2.902 9
0.1	3.089 4	3.191 0	3.205 3	3.198 6	3.176 8	3.147 2	3.108 2	3.068 0	3.026 5	2.985 0	–
0.2	3.162 1	3.206 8	3.215 8	3.207 4	3.192 1	3.165 8	3.132 7	3.095 7	3.060 9	–	–
0.3	3.174 8	3.196 2	3.207 0	3.202 6	3.190 8	3.172 2	3.145 0	3.113 8	–	–	–
0.4	3.143 6	3.174 7	3.189 8	3.190 8	3.185 6	3.170 8	3.150 6	–	–	–	–
0.5	3.103 8	3.145 9	3.166 0	3.173 2	3.170 9	3.163 8	–	–	–	–	–
0.6	3.063 1	3.110 8	3.137 4	3.149 9	3.155 3	–	–	–	–	–	–
0.7	3.035 3	3.073 4	3.105 8	3.123 4	–	–	–	–	–	–	–
0.8	2.983 6	3.033 9	–	–	–	–	–	–	–	–	–
0.9	2.948 6	–	–	–	–	–	–	–	–	–	–
1.0	2.870 9	–	–	–	–	–	–	–	–	–	–

Note: – represents no data.

Table 6. Regional reliability index (T = 50 a)

a_1	a_2										
	0	0.1	0.2	0.3	0.4	0.5	0.6	0.7	0.8	0.9	1.0
0	2.499 2	2.891 2	2.953 2	2.946 8	2.928 4	2.889 4	2.834 9	2.795 5	2.754 0	2.710 4	2.674 3
0.1	2.870 5	2.967 2	2.992 3	2.979 5	2.948 4	2.914 8	2.872 8	2.833 3	2.790 0	2.748 8	–
0.2	2.949 2	2.989 0	3.000 8	2.985 7	2.958 5	2.935 8	2.898 5	2.861 9	2.817 7	–	–
0.3	2.947 0	2.980 8	2.986 0	2.983 4	2.967 2	2.945 9	2.914 0	2.878 4	–	–	–
0.4	2.919 7	2.956 6	2.970 1	2.973 4	2.958 8	2.944 0	2.921 4	–	–	–	–
0.5	2.881 1	2.927 0	2.946 7	2.954 5	2.951 3	2.931 9	–	–	–	–	–
0.6	2.835 3	2.890 9	2.917 5	2.929 7	2.931 0	–	–	–	–	–	–
0.7	2.799 6	2.848 8	2.884 4	2.902 3	–	–	–	–	–	–	–
0.8	2.761 0	2.809 1	–	–	–	–	–	–	–	–	–
0.9	2.711 6	–	–	–	–	–	–	–	–	–	–
1.0	2.658 4	–	–	–	–	–	–	–	–	–	–

Note: – represents no data.

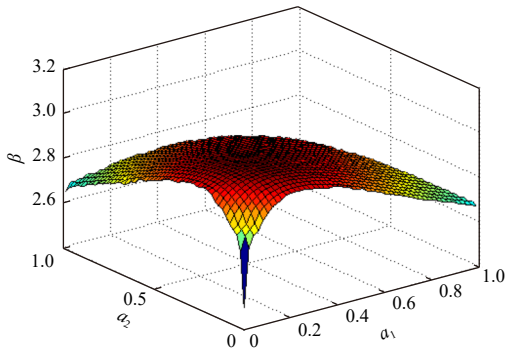

Fig. 9. Regional reliability index (T = 50 a).

6 Conclusions

According to four types of univariate probability distributions and four types of trivariate copulas, the optimal marginal and joint distribution functions of *VI*, *RI*, and *LI* were selected through K-S tests and AIC values. The joint return periods of *VI*, *RI*, and *LI* during a tropical cyclone were determined to evaluate the joint hazard-causing intensity. The interannual variation of the trivariate joint return period for 129 historical tropical cyclones was analysed. Finally, by constructing the limit state function of Hong Kong's resistance to tropical cyclones, the regional reliability of Hong Kong under tropical cyclones was evaluated.

The results indicated that the joint return period of *VI*, *RI*, and *LI* can reflect the joint hazard-causing intensity of strong wind, heavy rain, and storm surge caused by tropical cyclones. In the analysis of the interannual variation of the comprehensive hazard-causing intensity of tropical cyclones (excluding Super Typhoon Mangkhut), the annual, maximum, and average annual hazard-causing intensities of tropical cyclones exhibited obvious periodic change, and the period was approximately 9 a. Without considering the Super Typhoon Mangkhut, the maximum value of each cycle exhibited a decreasing trend.

According to the calculation of the regional reliability index of tropical cyclones affecting Hong Kong, if the return periods of the overall design of the regional structures decrease, the regional ability to defend against tropical cyclone disasters will be degraded.

Acknowledgements

Thanks to Shuntao Fan, Jialing Song and Haoshuang Song for their help in data collation.

References

Bloemendaal N, Muis S, Haarsma R J, et al. 2019. Global modeling of tropical cyclone storm surges using high-resolution forecasts. Climate Dynamics, 52(7): 5031–5044, doi: 10.1007/s00382-018-4430-x

Cerveny R S, Newman L E. 2000. Climatological relationships between tropical cyclones and rainfall. Monthly Weather Review, 128(9): 3329–3336, doi: 10.1175/1520-0493(2000)128<3329:CRBTCA>2.0.CO;2

Chen Peiyan, Yang Yuhua, Lei Xiaotu, et al. 2009. Cause analysis and preliminary hazard estimate of typhoon disaster in China. Journal of Natural Disasters (in Chinese), 18(1): 64–73

Chen Peiyan, Yu Hui, Xu Ming, et al. 2019. A simplified index to assess the combined impact of tropical cyclone precipitation and wind on China. Frontiers of Earth Science, 13(4): 672–681, doi: 10.1007/s11707-019-0793-5

Czajkowski J, Villarini G, Michel-Kerjan E, et al. 2013. Determining tropical cyclone inland flooding loss on a large scale through a new flood peak ratio-based methodology. Environmental Research Letters, 8(4): 044056, doi: 10.1088/1748-9326/8/4/044056

Ding Yifan, Liu Jiping, Chen Shengzhe, et al. 2020. Uniqueness of Lekima compared to tropical cyclones landed in the east coast of China during 1979–2019. Acta Oceanologica Sinica, 39(8): 121–124, doi: 10.1007/s13131-020-1639-4

Hendricks E A. 2012. Internal dynamical control on tropical cyclone intensity variability—A review. Tropical Cyclone Research and Review, 1(1): 97–105, doi: 10.6057/2012TCRR01.11

Hong Kong Observatory. 1997–2020. Tropical cyclone annual publications (in Chinese). https://www.hko.gov.hk/sc/publica/pubtc.htm [2022-11-17]

Hoque M A A, Phinn S, Roelfsema C, et al. 2017. Tropical cyclone disaster management using remote sensing and spatial analysis: A review. International Journal of Disaster Risk Reduction, 22: 345–354, doi: 10.1016/j.ijdrr.2017.02.008

Houze Jr R A. 2014. Clouds and precipitation in tropical cyclones. International Geophysics, 104: 287–327, doi: 10.1016/B978-0-12-374266-7.00010-X

Hu Siyi, Wang Zongzhi, Wang Yintang, et al. 2010. Encounter probability analysis of typhoon and plum rain in the Taihu Lake Basin. Science China: Technological Sciences, 53(12): 3331–3340, doi: 10.1007/s11431-010-4158-2

Kashem M, Ahmed M K, Qiao Fangli, et al. 2019. The response of the upper ocean to tropical cyclone Viyaru over the Bay of Bengal. Acta Oceanologica Sinica, 38(1): 61–70, doi: 10.1007/s13131-019-1370-1

Kim S, Pan Shunqi, Mase H. 2019. Artificial neural network-based storm surge forecast model: Practical application to Sakai Minato, Japan. Applied Ocean Research, 91: 101871, doi: 10.1016/j.apor.2019.101871

Kruk M C, Gibney E J, Levinson D H, et al. 2010. A climatology of inland winds from tropical cyclones for the eastern United States. Journal of Applied Meteorology and Climatology, 49(7): 1538–1547, doi: 10.1175/2010JAMC2389.1

Li Qingqing, Duan Yihong. 2010. Tropical cyclone strikes at the coastal cities of China from 1949 to 2008. Meteorology and Atmospheric Physics, 107(1): 1–7, doi: 10.1007/s00703-010-0065-0

Li Ning, Liu Xueqin, Xie Wei, et al. 2013. The return period analysis of natural disasters with statistical modeling of bivariate joint probability distribution. Risk Analysis, 33(1): 134–145, doi: 10.1111/j.1539-6924.2012.01838.x

Lin-Ye J, García-León M, Gràcia V, et al. 2017. Multivariate statistical modelling of future marine storms. Applied Ocean Research, 65: 192–205, doi: 10.1016/j.apor.2017.04.009

Liu Xueqin, Li Ning, Yuan Shuai, et al. 2015. The joint return period analysis of natural disasters based on monitoring and statistical modeling of multidimensional hazard factors. Science of the Total Environment, 538: 724–732, doi: 10.1016/j.scitotenv.2015.08.093

Melton G, Gall M, Mitchell J T, et al. 2010. Hurricane Katrina storm surge delineation: implications for future storm surge forecasts and warnings. Natural Hazards, 54(2): 519–536, doi: 10.1007/s11069-009-9483-z

Meyer R J, Baker J, Broad K, et al. 2014. The dynamics of hurricane risk perception: real-time evidence from the 2012 Atlantic hurricane season. Bulletin of the American Meteorological Society, 95(9): 1389–1404, doi: 10.1175/BAMS-D-12-00218.1

Mirabbasi R, Fakheri-Fard A, Dinpashoh Y. 2012. Bivariate drought frequency analysis using the copula method. Theoretical and Applied Climatology, 108(1–2): 191–206, doi: 10.1007/s00704-011-0524-7

Phadke A C, Martino C D, Cheung K F, et al. 2003. Modeling of tropical cyclone winds and waves for emergency management. Ocean Engineering, 30(4): 553–578, doi: 10.1016/S0029-8018(02)00033-1

Radfar S, Shafieefar M, Akbari H, et al. 2021. Design of a rubble mound breakwater under the combined effect of wave heights and water levels, under present and future climate conditions. Applied Ocean Research, 112: 102711, doi: 10.1016/j.apor.2021.102711

Saha K K, Wasimi S A. 2014. An index to assess the propensity of landfall in Australia of a tropical cyclone. Natural Hazards, 72(2): 1111–1121, doi: 10.1007/s11069-014-1058-y

Schroeder J L, Edwards B P, Giammanco I M. 2009. Observed tropical cyclone wind flow characteristics. Wind and Structures, 12(4): 349–381, doi: 10.12989/was.2009.12.4.349

Shao Zhuxiao, Liang Bingchen, Li Huajun, et al. 2018. Blended wind fields for wave modeling of tropical cyclones in the South China Sea and East China Sea. Applied Ocean Research, 71: 20–33, doi: 10.1016/j.apor.2017.11.012

Shi Xianwu, Yu Pubing, Guo Zhixing, et al. 2020. Simulation of storm surge inundation under different typhoon intensity scenarios: case study of Pingyang County, China. Natural Hazards and Earth System Sciences, 20(10): 2777–2790, doi: 10.5194/nhess-20-2777-2020

Sklar A. 1959. Fonctions de répartition à n dimensions et leurs marges. Paris: Publications de l'Institut de Statistique de l'Université de Paris, 229–231

Sun Zhilin, Huang Senjun, Nie Hui, et al. 2015. Risk analysis of seawall overflowed by storm surge during super typhoon. Ocean Engineering, 107: 178–185, doi: 10.1016/j.oceaneng.2015.07.041

Tsakiris G, Kordalis N, Tsakiris V. 2015. Flood double frequency analysis: 2D-Archimedean Copulas vs bivariate probability distributions. Environmental Processes, 2(4): 705–716, doi: 10.1007/s40710-015-0078-2

Wang Cao, Zhang Hao. 2018. Probability-based estimate of tropical cyclone damage: An explicit approach and application to Hong Kong, China. Engineering Structures, 167: 471–480, doi: 10.1016/j.engstruct.2018.04.064

Xiao Fengjin, Yin Yizhou, Luo Yong, et al. 2011. Tropical cyclone hazards analysis based on tropical cyclone potential impact index. Journal of Geographical Sciences, 21(5): 791–800, doi: 10.1007/s11442-011-0880-3

Xu Hongshi, Xu Kui, Lian Jijian, et al. 2019. Compound effects of rainfall and storm tides on coastal flooding risk tochastic. Stochastic Environmental Research and Risk Assessment, 33(7): 1249–1261, doi: 10.1007/s00477-019-01695-x

Yan Zhiduo, Wu Guoxiang, Liang Bingchen, et al. 2020. A stochastic tropical cyclone model for the northwestern Pacific Ocean with improved track and intensity representations. Applied Ocean Research, 105: 102423, doi: 10.1016/j.apor.2020.102423

Ye Yanting, Fang Weihua. 2018. Estimation of the compound hazard severity of tropical cyclones over coastal China during 1949–2011 with copula function. Natural Hazards, 93(2): 887–903, doi: 10.1007/s11069-018-3329-5

Yu Jinhua, Xue Huaxing, Song Jie. 2017. Tropical cyclone potential hazard in Southeast China and its linkage with the East Asian westerly jet. Asia-Pacific Journal of Atmospheric Sciences, 53(2): 295–304, doi: 10.1007/s13143-017-0028-1

Yussouf N, Jones T A, Skinner P S. 2020. Probabilistic high-impact rainfall forecasts from landfalling tropical cyclones using Warn-on-Forecast system. Quarterly Journal of the Royal Meteorological Society, 146(730): 2050–2065, doi: 10.1002/qj.3779